



DOI: 10.22144/ctu.jen.2016.109

## DATA PROCESSING FOR GROUND PENETRATING RADAR USING THE CONTINUOUS WAVELET TRANSFORM

Duong Quoc Chanh Tin<sup>1</sup> and Duong Hieu Dau<sup>2</sup>

<sup>1</sup>School of Education, Can Tho University, Vietnam

<sup>2</sup>College of Natural Science, Can Tho University, Vietnam

---

### ARTICLE INFO

Received date: 23/08/2015

Accepted date: 08/08/2016

---

### KEYWORDS

*Ground penetrating radar, continuous wavelet transform, detecting underground targets, multiscale edge detection*

---

### ABSTRACT

*Wavelet transform is one of the new signal analysis tools, plays an important role in numerous areas like image processing, graphics, data compression, gravitational and geomagnetic data processing, and some others. In this study, we use the continuous wavelet transform (CWT) and the multiscale edge detection (MED) with the appropriate wavelet functions to determine the underground targets. The results for this technique from the testing on five theoretical models and experimental data indicate that this is a feasible method for detecting the sizes and positions of the anomaly objects. This GPR analysis can be applied for detecting the natural resources in research shallow structure.*

Cited as: Tin, D.Q.C. and Dau, D.H., 2016. Data processing for ground penetrating radar using the continuous wavelet transform. Can Tho University Journal of Science. Vol 3: 85-93.

### 1 INTRODUCTION

Ground Penetrating Radar (GPR) has been a kind of rapid developed equipment in recent years. It is one of useful means to detect underground targets with many advantages, for example, non-destructive, fast data collection, high precision and resolution. It is currently widely used in research shallow structure such as: forecast landslide, subsidence, mapping urban underground works, traffic, construction, archaeology and other various fields of engineering. Therefore, the method for GPR data processing has been becoming increasingly urgent.

GPR data processing and analyzing takes a lot of time because it has many stages such as: data format, topographic correction, denoising, amplification and some others (Nguyen Thanh Van and Nguyen Van Giang, 2013). In final analysis step, the researchers need to detect there crucial param-

ters: position, size of the singular objects and buried depth – the distances between the ground and top surface of the objects.

Size determination of buried objects by GPR using traditional methods has many difficulties since it depend on electromagnetic wave propagation velocity in the material environment ( $v$ ), and this velocity varies very complex in all different directions. Recently, Sheng and his colleagues (2010) used the discrete wavelet transform (DWT) to filter and enhance the GPR raw data in order to obtain higher quality profile image. However, the interpretative results in that study still counted on  $v$ . In addition, the experimental models were built quite ideal – the unified objects in the unified environment. Thus, the study was only done in the laboratory, it is difficult to apply to the real data.

The continuous wavelet transform has becoming a very useful tool in geophysics (Ouadfeul, 2010). In potential field analysis it was used to locate and

characterize the anomaly sources (Dau, 2013). By clear and careful analysis, we recognize that the GPR data structure is quite similar to potential field data structure not only form but also nature. Therefore, a new technique to process GPR data using continuous wavelet transform on GPR signals is applied. The data is denoised by the line weight function (Fiorentine and Mazzantini, 1966), and then combine with the multiscale edge detection method (Dau *et al.*, 2007) to determine the size and position of the buried pipe, without consider the speed of an electromagnetic wave in the survey environment.

We start firstly by giving the theoretical background of the ground penetrating radar, the continuous wavelet transform and wavelet Poisson – Hardy function, the multiscale edge detection, the line weight function as well as the process for GPR data analysis using the wavelet transform. After that, the technique has been tested on four theoretical models before applied on experimental model - the real GPR data of water supply pipe in Ho Chi Minh City.

## 2 THEORETICAL BACKGROUND

### 2.1 Ground Penetrating Radar

Using radar reflections to detect subsurface objects in the first was proposed by Cook, in 1960. Subsequently, Cook and other researchers (Moffatt and Puskar, 1976) continued to develop radar systems to discover reflections beneath the ground surface. The fundamental theory of ground penetrating radar was described in detail by Benson (1995). In short, GPR system sends out pulses of electromagnetic wave into the ground, typically in the 10-2000 MHz frequency range, travels away from the source with the velocity depend on material structure of the environment. When the radar wave moves, if it meets anomaly objects or layers with different electromagnetic characteristics, a part of the wave energy will reflect or scatter back to the ground. The remaining energy continues to pass into the ground to be further reflected, until it finally spreads or dissipates with depth. The reflective wave is detected by receiver antenna and saved into memory of the device to analyze and process. The traces along a transect profile are stacked vertically; they can be viewed as two-dimensional vertical reflection profiles of the subsurface stratigraphy or other buried features. When the object is in front of the antenna, it takes more time for the radar waves to bounce back to the antenna. As the antenna passes over the object, the reflection time becomes shorter, and then longer again as it goes past the object. This effect causes the image to take the shape of a curve, called a “hyperbola”. This

hyperbola is actually the image of a smaller object (like a pipe) located at the center of the curve (Fig. 2a, 3a, 4a, 6a, 7a).

The speed of an electromagnetic wave ( $v$ ) in a material is given by (Sheng *et al.*, 2010):

$$v = \frac{c}{\sqrt{\left(\frac{\epsilon_r \mu_r}{2}\right)\left(\left(1 + P^2\right)^{\frac{1}{2}} + 1\right)}} \quad (1)$$

where  $P$  shows the loss factor, it leans on the frequency of the electromagnetic wave, and is a function of conductivity and permittivity of the medium,  $c = 0.2998 \text{ m/ns}$  is the speed of light in the vacuum,  $\epsilon_r$  indicates the relative dielectric constant,  $\mu_r$  illustrates the relative magnetic permeability ( $\mu_r = 1.0$  for non-magnetic materials).

The depth of penetration ( $h$ ) can be defined by correlating the velocity of the medium and the travelling time of the GPR signals. This allows the use of the following equation (Sheng, *et al*, 2010):

$$h = \frac{\sqrt{(t.v)^2 - S^2}}{2} \quad (2)$$

where  $S$  is the fixed distance between the transmitting and receiving antennas of the GPR system.

### 2.2 Continuous wavelet transform and wavelet Poisson – Hardy function

The continuous wavelet transform of 1-D signal  $f(x) \in L^2(R)$  can be given by:

$$W(s, b) = \frac{1}{\sqrt{s}} \int_{-\infty}^{+\infty} f(x) \overline{\psi} \left( \frac{b-x}{s} \right) dx = \frac{1}{\sqrt{s}} (f * \overline{\psi}) \quad (3)$$

Where,  $s, b \in R^+$  are scale and translation (shift) parameters, respectively;  $L^2(R)$  is the Hilbert space of 1-D wave functions having finite energy;  $\overline{\psi}(x)$  is the complex conjugate function of  $\psi(x)$ , an analyzing function inside the integral (3),  $f * \overline{\psi}$  expresses convolution integral of  $f(x)$  and  $\overline{\psi}(x)$ . In particularly, CWT can operate with various complex wavelet functions, if the wavelet function curve looks like the same form of the original signal.

To determine the boundary from anomaly objects, and then estimate their size and location, we use Poisson-Hardy complex wavelet function that was designed by Duong Hieu Dau (Duong Hieu Dau, *et al*, 2007). It is given by:

$$\psi^{(PH)}(x) = \psi^{(P)}(x) + i\psi^{(H)}(x) \quad (4)$$

$$\text{where, } \psi^{(P)}(x) = -\frac{2}{\pi} \cdot \frac{1-3x^2}{(1+x^2)^3} \quad (5)$$

$$\psi^{(H)}(x) = \text{Hilbert}(\psi^{(P)}(x)) = \frac{2}{\pi} \cdot \frac{-3x+x^3}{(1+x^2)^3} \quad (6)$$

### 2.3 Multiscale edge detection

In image processing, determination of the edge is a considerable task. According to image processing theory, the edges of image are areas with rapidly changing light intensity or color contrast sharply. For the signal varies in the space, like GPR signal, the points where the amplitude of the signal quickly or suddenly changing are considered to the boundaries. Application of the image processing theory to analyze GPR data, determining the edges corresponding detecting the position and the relative size of the anomaly objects. To detect the boundary of singularly objects, the wavelet transform is operated with different scales, and the edges are a function of the scales. Accordingly, the edge detection method using wavelet transform is also called the “multiscale edge detection” technique (Dau *et al.*, 2007).

### 2.4 Line Weight Function (LWF)

Line Weight Function is the linear combination between Gaussian function and the function which is formed by the second derivative of Gaussian function (according to spatial variable) (Fiorentine and Mazzantini, 1966):

$$l\left(\frac{x}{\sigma}\right) = C_0 h_0\left(\frac{x}{\sigma}\right) + C_2 h_2\left(\frac{x}{\sigma}\right) \quad (7)$$

where, Gaussian function  $h_0\left(\frac{x}{\sigma}\right)$  has format:

$$h_0\left(\frac{x}{\sigma}\right) = \frac{1}{\sigma\sqrt{\pi}} \exp\left(-\frac{x^2}{2\sigma^2}\right) \quad (8)$$

and  $h_2\left(\frac{x}{\sigma}\right)$  indicates the second derivative of Gaussian function:

$$h_2\left(\frac{x}{\sigma}\right) = \frac{1}{\sqrt{8\pi\sigma^2}} \left( -\exp\left[-\frac{x^2}{2\sigma^2}\right] + \frac{x^2}{\sigma^2} \exp\left[-\frac{x^2}{2\sigma^2}\right] \right) \quad (9)$$

The line weight function effectively applies to de-noise as well as to enhance the contrast in the edges when using with MED and CWT technique (Dau, 2013).

### 2.5 The process for GPR data analysis using the wavelet transform

**Step 1:** Selecting an optimal GPR data slice to cut.

After processing the raw data, we are going to obtain a GPR section quite clear and complete. The sectional data is a matrix  $[m \times n]$  including  $m$  rows (corresponding to the number of samples per trace) and  $n$  columns (corresponding to the number of traces). The number of traces relies on the length of data collection route and the trace spacing ( $dx$ ). The number of samples per trace is decided by the depth of the survey area and the sampling interval ( $dt$ ). From the GPR section, an optimal data cutting layer is chosen (matching with a row in the matrix) to analyze by the wavelet method. Choosing this data cutting layer considerably depend on the experience of the researchers, they have to test with many different layers by theoretical models as well as experimental models. The edges of anomaly objects will be determined exactly, if an appropriate data slice is selected.

**Step 2:** Denoising data by the line weight function.

The appropriate data is denoised by the line weight function that increasingly supporting resolution in multiscale edge detection using the continuous wavelet transform.

**Step 3:** Handling unwanted data after the filtering.

The new data set after the filtering contains interpolated data near the boundary, and that is unwanted data. Therefore, we need to remove it to gain an adequate data.

**Step 4:** Performing Poisson - Hardy wavelet transform with GPR signals which were denoised by the line weight function.

After complex continuous wavelet transform, there are four distinct data sets: real part, virtual component, module factor, and phase ingredient. Module and phase data will be used in the next step.

**Step 5:** Changing the different scales ( $s$ ) and repeating the multiscale wavelet transform.

**Step 6:** Plotting the module contour and phase contour by the wavelet transform coefficients with different scales ( $s$ ).

The steps from 1 to 6 are operated by the modules program and run by Matlab software.

**Step 7:** Determining the size and location of the buried pipe.

The location of the buried pipe is detected by the plot of module contour:

$$x = \text{center coordinate} \times dx \quad (10)$$

The size of the buried pipe is detected by the plot of phase contour:

$$D = (\text{right edge coordinate} - \text{left edge coordinate}) \times dx \quad (11)$$

### 3 RESULTS AND DISCUSSIONS

#### 3.1 Theoretical models

To verify the reliability of the proposed method, our research group has tested on many different theoretical models including: the cylinders are made from various materials such as plastic, metal and concrete. The cylinders are also designed in numerous dissimilar sizes and their structures are very close to the actual models, and are buried in the distinct environment (from homogeneous to heterogeneous). The relative errors of the determination are within the permitted limits show that the

obtained results are reliable. However, in this paper, we only introduce typical treatment results with four plastic tube models having different sizes that the first three models are buried in homogeneous environments, and the fourth model is buried in heterogeneous environments.

##### 3.1.1 Model 1

Using antenna frequency 700 MHz, unified environment, dry sand has thickness 5.0 m, conductivity  $\sigma = 0.01 \text{ mS/m}$ ,  $\epsilon_r = 5.0$ ,  $\mu_r = 1.0$ ,  $v = 0.13 \text{ m/ns}$  (Van and Giang, 2013). Underneath anomaly object is the plastic tube:  $\sigma = 1.0 \text{ mS/m}$ ,  $\epsilon_r = 3.0$ ,  $\mu_r = 1.0$ ,  $v' = 0.17 \text{ m/ns}$ , inside contains the air; the center of the object is located at horizontal coordination  $x = 5.0 \text{ m}$  and vertical coordination  $z = 1.0 \text{ m}$ , inside pipe diameter  $d = 0.32 \text{ m}$ , outside pipe diameter  $D = 0.40 \text{ m}$ .

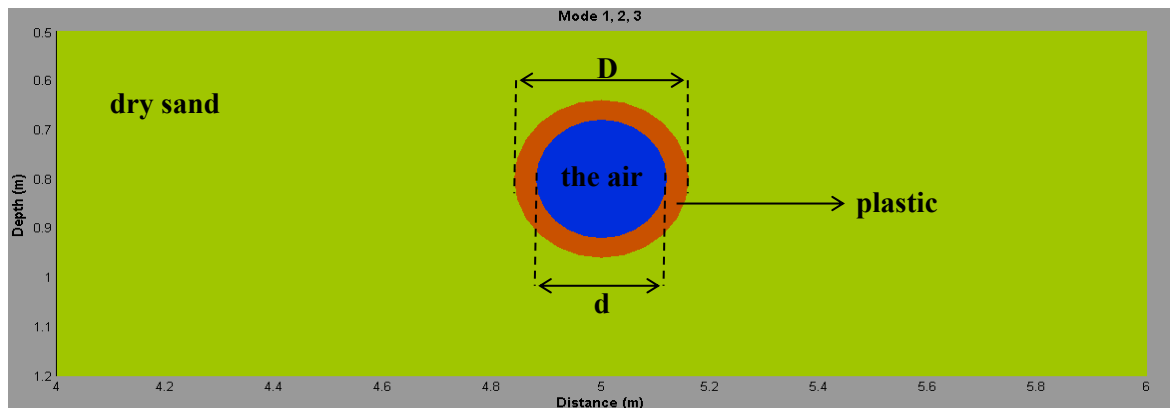


Fig. 1: Vertical section of the buried pipe in model 1, 2, 3

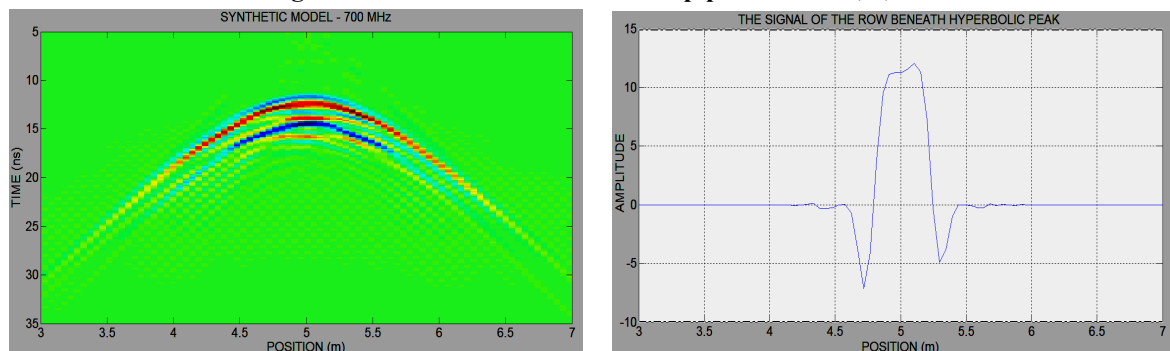
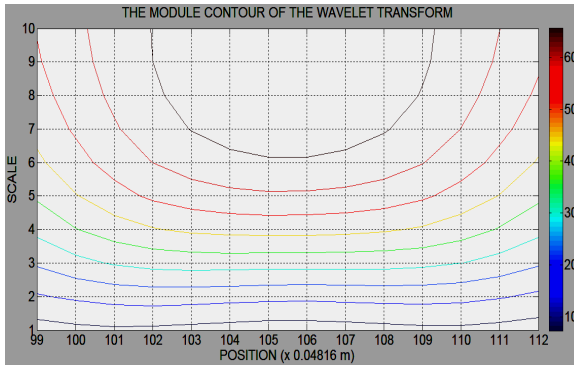


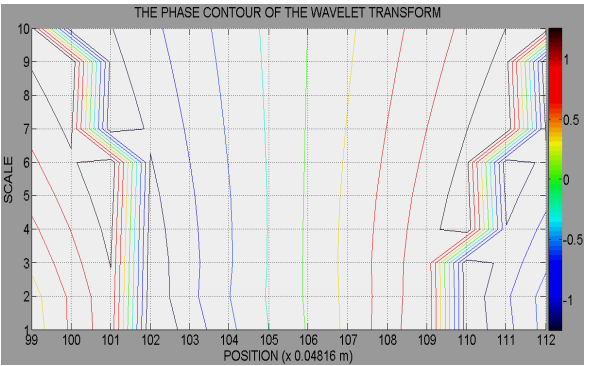
Fig. 2a: GPR section of the model 1

Fig. 2b: The signal of the row beneath hyperbolic peak



**Fig. 2c: The module contour of the wavelet transform**

According to the results plotting of the module in the figure 2c, we easily find the center of the anomaly object locating at 105.5. Moreover, the left edge and the right edge coordination of the anomaly object are presented at 101.5, 109.5 respectively in the figure 2d. So, we can determine the position and size of the pipe by the equation



**Fig. 2d: The phase contour of the wavelet transform**  
(10) and (11). The calculative results are represented in Table 1.

### 3.1.2 Model 2

The basic parameters of the model 2 are similar the model 1, but the center of the object is located at vertical coordination  $z = 0.8$  m, inside pipe diameter  $d = 0.24$  m, outside pipe diameter  $D = 0.32$  m.

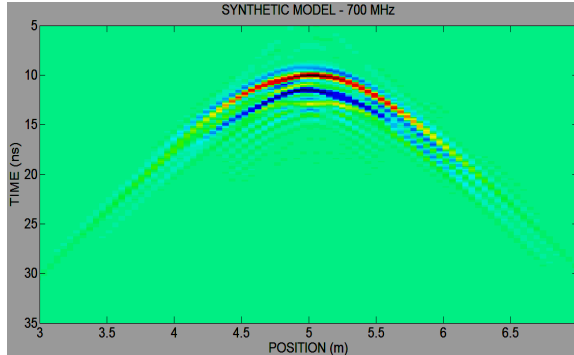


**Fig. 3a: GPR section of the model 2**

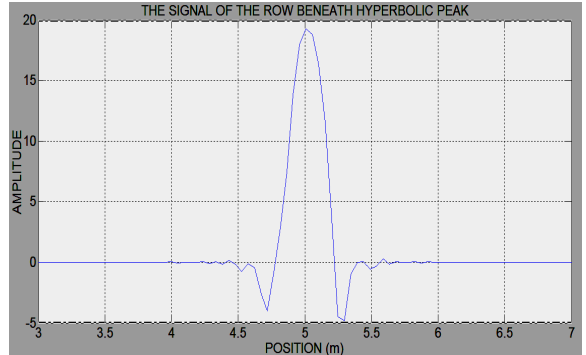


**Fig. 3b: The signal of the row beneath hyperbolic peak**

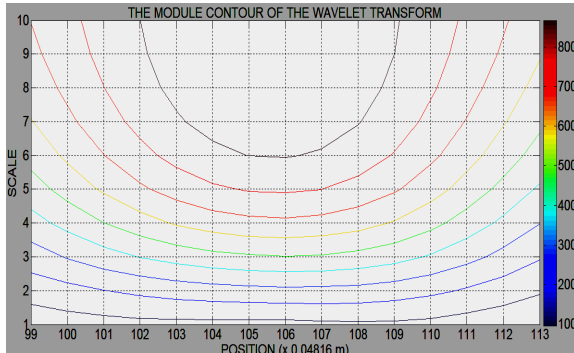


**Fig. 3c: The module contour of the wavelet transform**

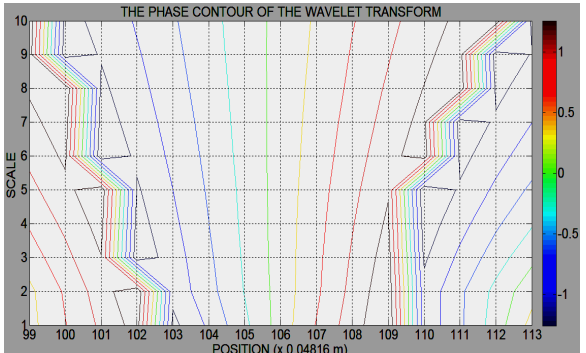


**Fig. 3d: The phase contour of the wavelet transform**

From the figure 3c and 3d, the center, the left edge and the right edge coordination of the anomaly object are clearly seen at 105.5, 102.5, 109.5 in turn. Therefore, the position and size of the pipe also are calculated by the same way in the model 1 (Table 1).

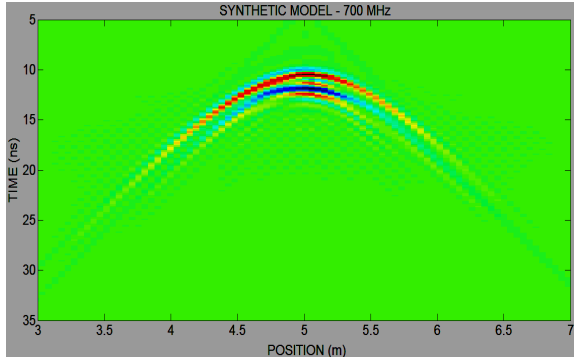


**Fig. 4a: GPR section of the model 3**

### 3.1.3 Model 3

The fundamental parameters of the model 3 are alike model 2, but the size of the object is different, inside pipe diameter  $d = 0.20$  m, outside pipe diameter  $D = 0.22$  m.

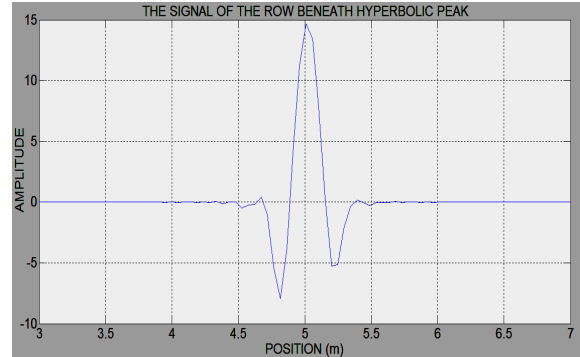


**Fig. 4b: The signal of the row beneath hyperbolic peak**

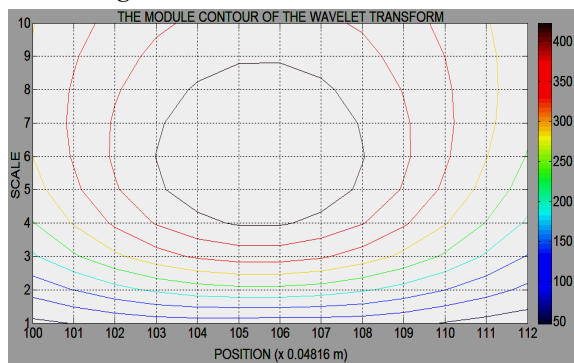


**Fig. 4c: The module contour of the wavelet transform**

The Figure 4c and 4d provide information on the center, the left edge and the right edge coordination of the anomaly object that are 105.5, 103.5, 108.5 respectively.

The interpretative results in table 1 show that the determining parameters of the pipes when they are buried in the homogeneous environment having high accuracy. With various sizes of the pipe, the relative error of the measurement is negative with the size. Specifically, the smaller in the size is the greater in the error.

Before applying to the actual data, we extendedly test on the next model to confirm the feasibility of the proposed method. The parameters of this model are built very close to the parameters of the real data.

#### 3.1.4 Model 4

Using antenna frequency 700 MHz, heterogeneous environment including three layers:

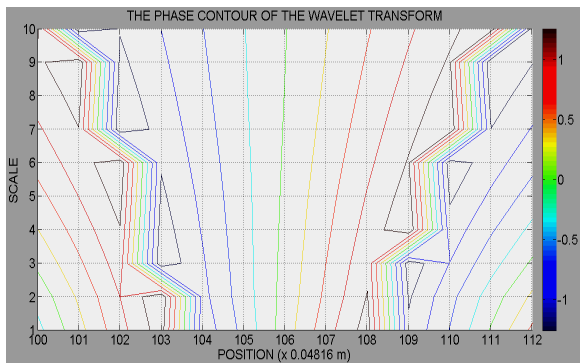


**Fig. 4d: The phase contour of the wavelet transform**

Layer 1: asphalt has thickness 0.2 m,  $\sigma = 0.001$  mS/m,  $\varepsilon_r = 4.0$ ,  $\mu_r = 1.0$ ,  $v_1 = 0.15$  m/ns.

Layer 2: breakstone has thickness 0.4 m,  $\sigma = 1.0$  mS/m,  $\varepsilon_r = 10.0$ ,  $\mu_r = 1.0$ ,  $v_2 = 0.10$  m/ns.

Layer 3: Clay soil has thickness 4.4 m,  $\sigma = 200$  mS/m,  $\varepsilon_r = 16.0$ ,  $\mu_r = 1.0$ ,  $v_3 = 0.07$  m/ns.

Underneath anomaly object is the plastic tube:  $\sigma = 1.0$  mS/m,  $\varepsilon_r = 3.0$ ,  $\mu_r = 1.0$ ,  $v' = 0.17$  (m/ns), inside contains the air; the center of the object is located at horizontal coordination  $x = 5.0$  m and vertical coordination  $z = 1.0$  m, inside pipe diameter  $d = 0.30$  m, outside pipe diameter  $D = 0.32$  m.

As can be seen in the figure 6c and 6d, the center, the left edge and the right edge coordination of the anomaly object are 134.0, 129.5, 138.5 in turn. The calculative results in table 1 illustrate that the detecting parameters of the pipe in model 4 when it is buried in the heterogeneous environment having noticeably low error (1.6% for position determining and 6.3% for size detecting).

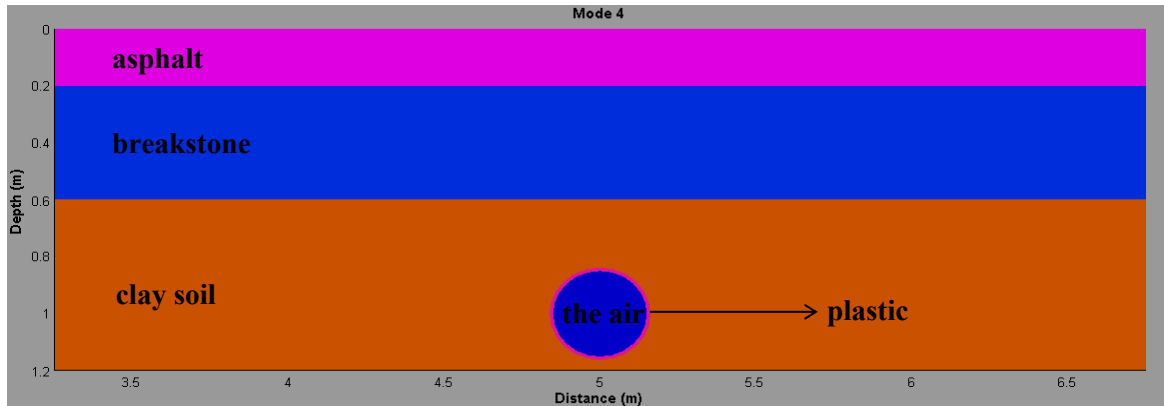


Fig. 5: Vertical section of the buried pipe in model 4

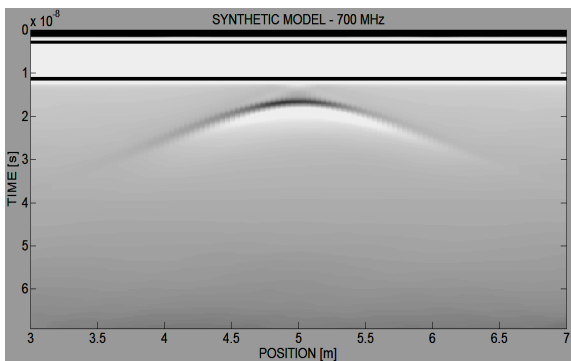


Fig. 6a: GPR section of the model 4

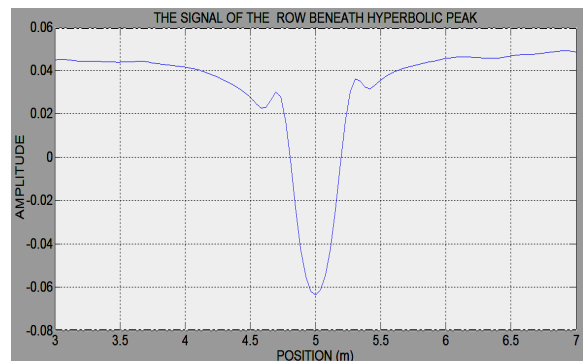


Fig. 6b: The signal of the row beneath hyperbolic peak

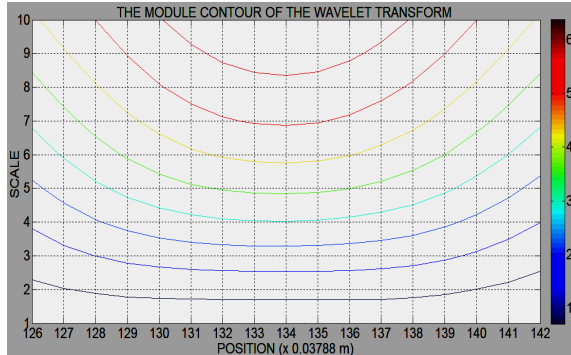


Fig. 6c: The module contour of the wavelet transform

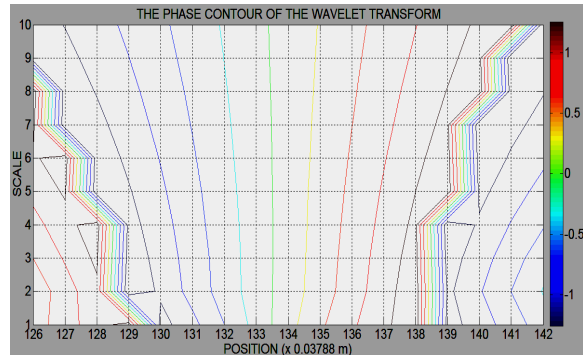


Fig. 6d: The phase contour of the wavelet transform

Table 1: Interpretative results of four theoretical models

Model no.	Position	Relative error	Size	Relative error
1	$x = 105.5 \times 0.04816 = 5.08 \text{ m}$	1.6%	$D = (109.5-101.5) \times 0.04816 = 0.39 \text{ m}$	3.7%
2	$x = 105.5 \times 0.04816 = 5.08 \text{ m}$	1.6%	$D = (109.5-102.5) \times 0.04816 = 0.34 \text{ m}$	6.3%
3	$x = 105.5 \times 0.04816 = 5.08 \text{ m}$	1.6%	$D = (108.5-103.5) \times 0.04816 = 0.24 \text{ m}$	9.5%
4	$x = 134.0 \times 0.03788 = 5.08 \text{ m}$	1.6%	$D = (138.5-129.5) \times 0.03788 = 0.34 \text{ m}$	6.3%

The accuracy of the proposed method is confirmed through the analysis of data on four theoretical models. The next job is going to apply this technique to analyze the actual GPR data which is measured by the team from Geophysics Department, Faculty of Physics and Engineering Physics, University of Science, VNU Ho Chi Minh City.

### 3.2 Experimental model – the water supply pipe

Data was measured by Duo detector (IDS, Italia), using antenna frequency 700 MHz. The route T84 was done in front of the house address A11, Nguyen Than Hien Street, District 4, Ho Chi Minh City on Monday, October 13, 2014 by the group from the Geophysics Department.

According to the information was provided by M.A.T limited liability company drainage works and urban infrastructure, the size of the buried pipe

is 0.2 m and it is located at horizontal coordination  $x = 2.0$  m along the survey route.

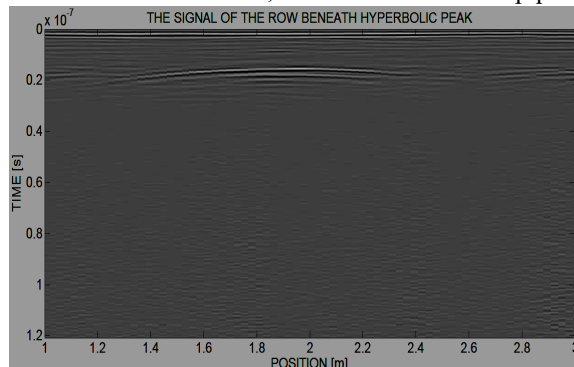


**Fig. 7a: GPR section of the water supply pipe data**

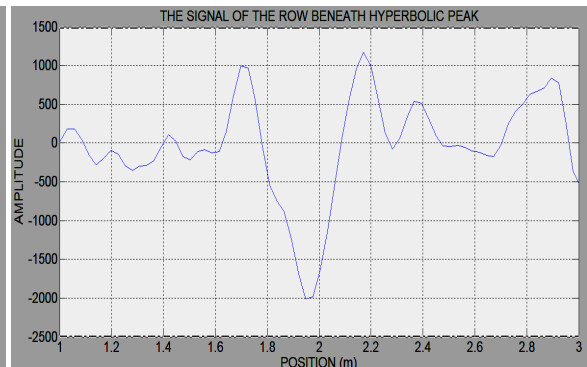


**Fig. 7b: The signal of the row beneath hyperbolic peak**

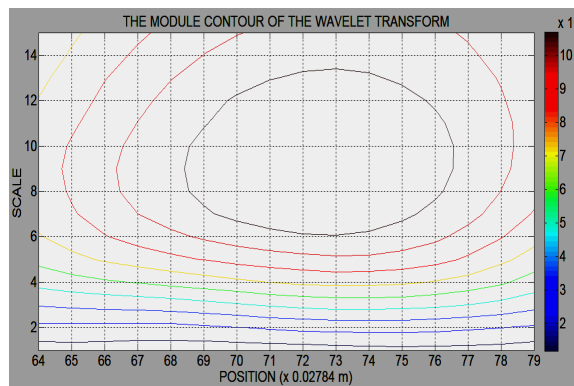


**Fig. 7c: The module contour of the wavelet transform**

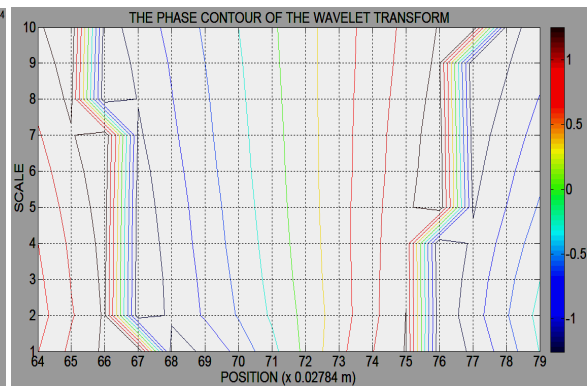


**Fig. 7d: The phase contour of the wavelet transform**

**Table 2: Interpretative results of experimental model**

Position	Relative error	Size	Relative error
$x = 72.5 \times 0.02784 = 2.02$ m	1.0%	$D = (75.5 - 67.5) \times 0.02784 = 0.22$ m	10.0%

The GPR data analysis bases on wavelet transform plays a major role for determination the location and size of the anomaly objects which are buried shallow in a heterogeneous environment, this could not be done by a radar machine itself. Then, for the next job to take out anomalies from the environment or put another pipeline into the ground. It is going to rather easier, saving constructive time and improving the economic efficiency.

#### 4 CONCLUSIONS

The GPR data interpretation process using continuous wavelet transform with Poisson – Hardy wavelet function to determine the position and the size of the anomaly objects is informed and applied. We test the process to analyze four theoretical models (three models corresponding three different size pipe are buried in the unified environment, and a model with the heterogeneous environment having three various layers), and an experimental model. Theoretical models are built

in this paper very close to the objects to be studied in practice in order to verify the reliability of the proposal method before application on the real data. The final results for the theoretical models in determining the location and the size have relative error 1.6% and from 3.7% (model 1) to 9.5% (model 3) in turn. For the experimental model, the relative error in detecting the position and the size are 1.0% and 10.0% respectively. There relevant results indicate that using continuous wavelet transform and multiscale edge detection technique provide an orientation to resolution ground penetrating radar data exceedingly efficient. If the researchers deeply combine the presentational technique and traditional methods to interpret GPR data, the identification of singularly bodies in shallow geologic study will be more effective.

#### ACKNOWLEDGMENTS

The authors would like to thank Ms. Nguyen Van Thuan for his help, and Prof. Nguyen Thanh Van

for his advices concerning the preparation of the paper and those reviewers for their constructive comments that improve the paper quality.

## REFERENCES

- Benson, A.K., 1995. Applications of ground penetrating radar in assessing some geological hazards—examples of groundwater contamination, faults, cavities. *Journal of Applied Geophysics*. 33: 177-193.
- Cook, J.C., 1960. Proposed monocycle-pulse VHF radar for airborne ice and snow measurements. *Journal of the American Institute of Electrical Engineers, Transactions on Communication and Electronics*. 79: 588-594.
- Dau, D.H., 2013. Interpretation of geomagnetic and gravity data using continuous wavelet transform. Vietnam National University Ho Chi Minh City Press. 127 pp.
- Dau, D.H., Chanh, T.C., Liet, D.V., 2007. Using the MED method to determine the locations and the depths of geomagnetic sources in the Mekong Delta. *Journal of Can Tho University*, 8: 21-27.
- Fiorente A., Mazzantini L., 1966. Neuron inhibition in the human fovea: A study of interaction between two line stimuli. *Atti della Fondazione Giorgio Ronchi*. 21: 738-747.
- Moffatt, D.L., Puskar, R.J., 1976. A subsurface electromagnetic pulse radar. *Geophysics*, 41: 506-518.
- Van, N.T., Giang, N.V., 2013. *Ground penetrating radar – Methods and Applications*. Vietnam National University Ho Chi Minh City Press. 222 pp.
- Ouadfeul, S., Aliouane, L., Eladj, S., 2010. Multiscale analysis of geomagnetic data using the continuous wavelet transform. Application to Hoggar (Algeria), *SEG Expanded Abstracts* 29, 1222-1225.
- Sheng, H.N., Yan, H.H., Kuo, F.L., Da, C.L., 2010. Buried pipe detection by ground penetrating radar using the discrete wavelet transform. *Elsevier, Computers and Geotechnics*, 37: 440-448.